Journal of Materials Chemistry

Cite this: *J. Mater. Chem.*, 2012, **22**, 17049

www.rsc.org/materials

PAPER

Controlled hydrothermal synthesis of 1D nanocarbons by surfactant-templated assembly for use as anodes for rechargeable lithium-ion batteries

Qiang Sun, Xiang-Qian Zhang, Fei Han, Wen-Cui Li and An-Hui Lu*

Received 13th May 2012, Accepted 2nd July 2012
DOI: 10.1039/c2jm33030j

In this study, we have developed a facile and controllable hydrothermal synthesis assisted by surfactant-templating and subsequent carbonization for low dimensional nanocarbons, particularly 1D rods/fibers. In this synthesis, resorcinol and hexamethylene tetramine (HMT) were used as the monomers and the surfactant Pluronic F127 as the structural directing agent. The nanostructures and morphologies of the as-synthesized carbon can be simply tailored by changing the concentrations of F127 and HMT. The obtained 1D nanocarbon structures with BET surface areas in the range of 570–585 $m^2\ g^{-1}$, markedly varied in shape from rods to fibers. When using these nanocarbon structures as the anode material for lithium ion batteries, it was found that carbon nanofibers demonstrated good rate performance (a high reversible capacity of 160 mA h g^{-1} at a current density of 1500 mA g^{-1} (*ca.* 4C)), which is much higher than that of the commercial artificial graphite. This high rate capability is attributed to the unique morphology of the carbon nanofibers with an average diameter of ~45 nm. Such thin and porous carbon fibers allow fast lithium ion transportation.

1 Introduction

Carbon nanorods/fibers, as representative 1D carbon nanostructures, are highly promising for applications in catalysis, adsorption, biomedicine, energy storage and conversion, due to their outstanding thermal stability, biocompatibility, electronic and mechanical properties.[1–10] As for their application in commercial lithium-ion batteries (LIBs), 1D nanocarbon structures not only provide shortened pathways for lithium ion transport, but also offer relatively large electrode/electrolyte interfaces to promote rapid charge-transfer reactions in LIBs. Thus, considerable efforts have been made in fabrication of 1D nanocarbon materials.[11–13] Some methods, such as electrospinning[5,7,13,14] and chemical vapor deposition (CVD),[15] have been used in the production of 1D carbon materials. However, it is very difficult to simultaneously achieve precise control over the properties of the resulting carbon materials in terms of surface area, pore size and shape. The template method is also a generally used approach for preparation of 1D carbon materials.[9,10,16–22] As pioneered by Holmes' group, well-aligned free-standing arrays of mesoporous carbon nanofibers have been fabricated on silicon wafers using anodic aluminum oxide membranes as templates.[21] Recently, Liang and co-workers synthesized a free-standing fibrous membrane using a hydrothermal carbonization (HTC) process from Te nanowires and glucose with the subsequent removal of the Te cores by H_2O_2.[22] The obtained carbon nanofibers were flexible and mechanically robust enough for filtration and separation of nanoparticles of different sizes from a solution. In this regard, the template method is considered a straightforward strategy to prepare 1D nanocarbons, while, it needs a multistep synthesis, which leads to a time-consuming procedure and low yield.[11,25] Hence, the key precondition to satisfy the demand for 1D nanocarbon materials is to explore a flexible and efficient synthesis which can produce the desired low dimensional nanocarbon materials with controlled morphology and tunable aspect ratio.

In this study, we report a facile and controllable hydrothermal synthesis assisted by surfactant-templating and a subsequent carbonization process for 1D nanocarbon materials. The synthesis strategy using easily available surfactants as structure-directing agents and resorcinol/formaldehyde (RF) resin as the carbon source provides a simple and efficient approach for the consecutive fabrication of low dimensional nanocarbon materials including carbon nanospheres and carbon rods/fibers, simply by varying the concentrations of surfactant F127 and reactant hexamethylene tetramine (HMT). To our knowledge, there has not been any similar report on such organized carbon fibers with detectable mesostructures in the literature. Importantly, the obtained carbon nanofibers have demonstrated good rate performance, *e.g.* when used as the anode material for lithium ion batteries.

State Key Laboratory of Fine Chemicals, School of Chemical Engineering, Faculty of Chemical, Environmental and Biological Science and Technology, Dalian University of Technology, Dalian 116024, P.R. China. E-mail: anhuilu@dlut.edu.cn; Fax: +86-411-84986112; Tel: +86-411-84986112

2 Experimental

2.1 Chemicals

Resorcinol (R, 99.5%), hexamethylene tetramine (HMT), NH_4OH (25 wt%), and formaldehyde (F, 37 wt%) were obtained from Sinopharm Chemical Reagent Co., Ltd. Pluronic F127 was purchased from Fluka. Commercial artificial graphite was purchased from Greentech Advanced Materials Co. Ltd. All chemicals were used as received.

2.2 The synthesis of polymer and carbon nanomaterials

The detailed synthesis conditions and textural parameters of the obtained nanocarbons were listed in Table 1. Typically, resorcinol (0.275 g, 2.5 mmol) and HMT (0.105 g, 0.75 mmol or 0.210 g, 1.5 mmol) were dissolved in deionized water (60 mL) with slow stirring. An amount of F127 (*e.g.* 200, 400, 800, and 1200 mg) was dissolved in 40 mL of deionized water. The two solutions were then mixed and kept stirring for 30 min. Finally the mixture solution was transferred into an autoclave and hydrothermally treated at 120 °C for 4 h, and a colloidal suspension was obtained. The resulting samples were retrieved by centrifugation (12 000 rpm, 5 min), washed with deionized water and ethanol, dried at 50 °C for 6 h. Carbon products were obtained by pyrolysis of the polymeric materials at 600 °C for 2 h under a nitrogen atmosphere.

2.3 Electrochemical measurements

Electrochemical experiments were performed *via* CR2025 coin-type test cells assembled in an argon-filled glove box with lithium metal as the counter and reference electrodes at room temperature. To prepare working electrodes, a mixture of active material, conductive carbon black and LA133 (water-based binder, Indigo) in water at a weight ratio of 80 : 10 : 10 was pasted on rough Cu foil with Celgard 2400 membrane as the separator to isolate electrons. The graphite electrode consisting of commercial artificial graphite was prepared with same weight ratio. The electrolyte consists of a solution of 1 M $LiPF_6$ in dimethyl carbonate (DMC), ethyl methyl carbonate (EMC) and ethylene carbonate (EC) (1 : 1 : 1 v/v/v) with 2 wt% fluorinated ethylene carbonate (FEC) as an additive. The discharge–charge measurements were carried out at different current densities of 100–1500 mA g^{-1} between 0.005 and 3 V on a Land CT2001A battery test system. Electrochemical impedance spectra (EIS) were performed on a CHI660D electrochemical workstation.

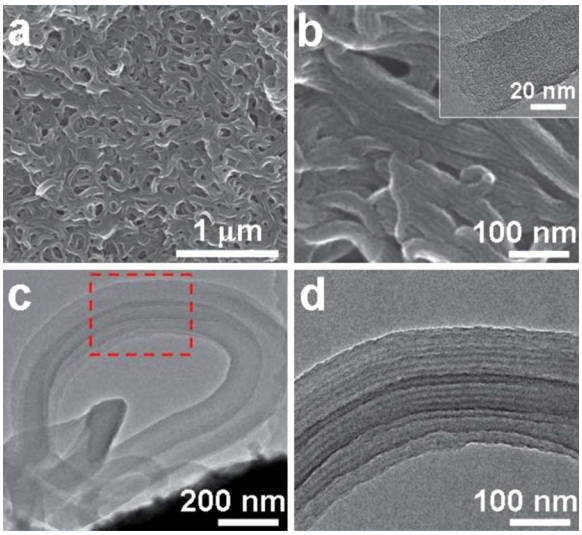

Fig. 1 SEM images (a and b) of CRF-1, TEM images (c and d) of PRF-1; inset shows the TEM image of CRF-1.

2.4 Characterization

Scanning electron microscopy (SEM) investigations were carried out with a FEI Nova NanoSEM 450 instrument. Transmission electron microscopy (TEM) analyses were carried out with Tecnai $G^2$20S-Twin equipment operating at 200 kV. The samples for TEM analysis were prepared by dropping an ethanol droplet of the products on carbon-coated copper grids and drying at room temperature. Nitrogen adsorption isotherms were measured with a Micromeritics ASAP 2020 adsorption analyzer at 77 K. Before the measurements, all the samples were degassed at 200 °C for 6 h. The specific surface areas (S_{BET}) were calculated from the adsorption data in the relative pressure range of 0.05 to 0.3 using the Brunauer–Emmett–Teller (BET) method. The total pore volume (V_{total}) was estimated from the amount adsorbed at a relative pressure of 0.90. Thermogravimetric analysis (TG) was conducted on a thermogravimetric analyzer STA 449 F3 with a heating rate of 10 °C min^{-1}.

Table 1 Synthesis conditions and texture parameters of the nanocarbon materials

	Synthesis conditions[a]					Texture parameters	
	Amount [mmol]						
Sample	R	HMT	F127	NH_4OH	F	S_{BET} (m^2 g^{-1})	V_{total} (cm^3 g^{-1})
CRF-1	2.5	1.50	0.0636	—	—	585	0.348
CRF-2	2.5	0.75	0.0159	—	—	582	0.302
CRF-3	2.5	0.75	0.0318	—	—	—	—
CRF-4	2.5	0.75	0.0636	—	—	570	0.300
CRF-5	2.5	0.75	0.0945	—	—	—	—
CRF-6	2.5	0.75	0.0636	3.0	—	—	—
PRF-7[b]	2.5	0.75	0.0636	—	4.5	—	—

[a] The samples were prepared by a hydrothermal process at 120 °C for 4 h in 100 mL water solution followed by carbonization at 600 °C. [b] PRF-7 was the polymeric product.

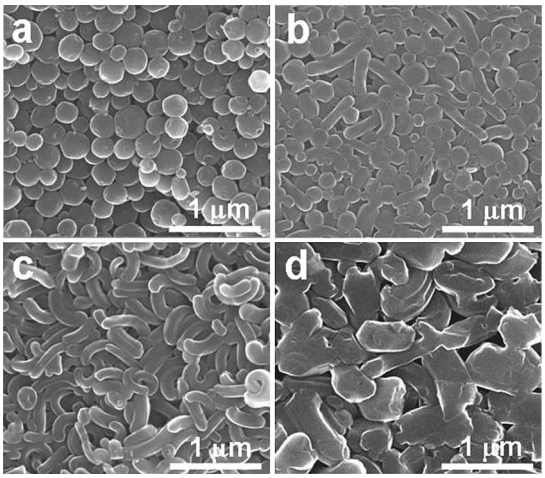

Fig. 2 SEM images of the carbon products: (a) CRF-2, (b) CRF-3, (c) CRF-4 and (d) CRF-5.

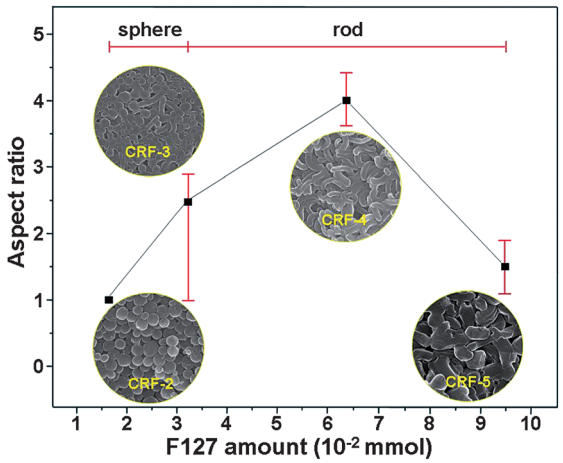

Fig. 3 Variation in morphology and aspect ratio of the as-synthesized carbon materials as a function of F127 amount.

3 Results and discussion

The solution-phase hydrothermal synthesis offers a remarkable opportunity for the molecular design of carbon morphologies, which is beneficial for enhancing lithium ion storage activity. Meanwhile, to provide shortened pathways for lithium ion transport, it is necessary to flexibly control the aspect ratio of 1D nanocarbons. Under this consideration, we herein attempt to introduce surfactant Pluronic F127 to the reaction system to direct the formation of 1D nanocarbons (denoted CRF, the corresponding polymer products denoted PRF). The as-prepared carbon nanofibers CRF-1 were characterized by SEM and TEM. As seen in Fig. 1a, CRF-1 is composed of carbon nanofibers with an average width of *ca.* 45 nm. The high resolution SEM (HRSEM) image of CRF-1 (Fig. 1b) shows the remarkable presence of long and narrow grooves on the exposed surface. Surprisingly, the TEM image (Fig. 1b inset) of CRF-1 reveals worm-like pores. In addition, the as-synthesized polymer fibers PRF-1 were characterized by TEM. As seen in Fig. 1c and d, the TEM images show 1D channels along the fibers growth

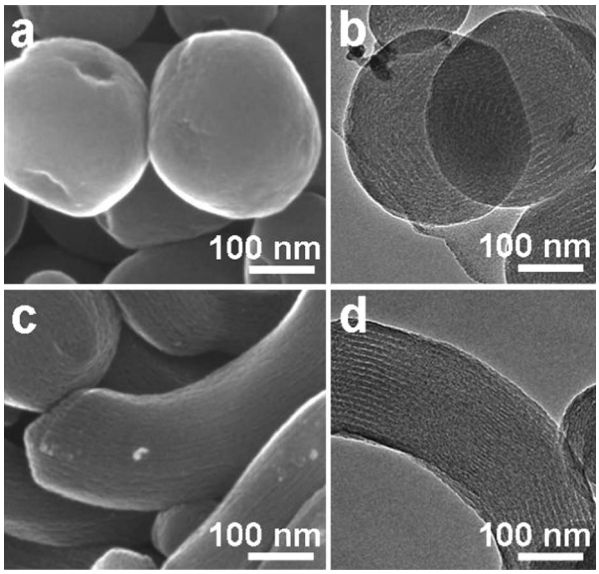

Fig. 4 SEM and TEM images of the carbon products: (a and b) CRF-2, (c and d) CRF-4.

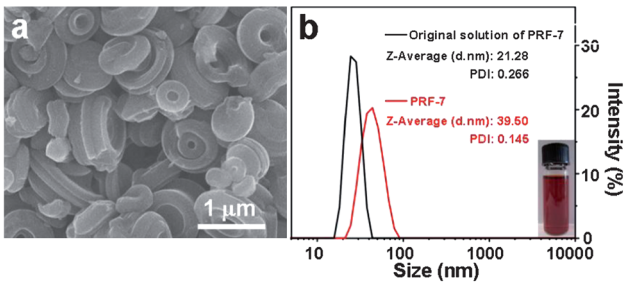

Fig. 5 SEM image (a) of CRF-6, DLS curves (b) of PRF-7 and its original solution (PDI = polydispersity index), inset showing the photograph of PRF-7.

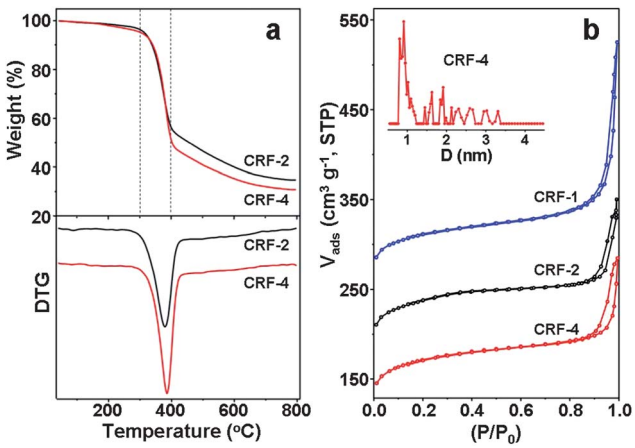

Fig. 6 TG and DTG curves of (a) CRF-2, and CRF-4; N_2 sorption isotherms (b) of CRF-1, CRF-2, and CRF-4, the isotherms of CRF-1, and CRF-2, are offset vertically by 140, and 70 $cm^3\ g^{-1}$, STP, respectively; inset showing DFT pore size distribution of CRF-4.

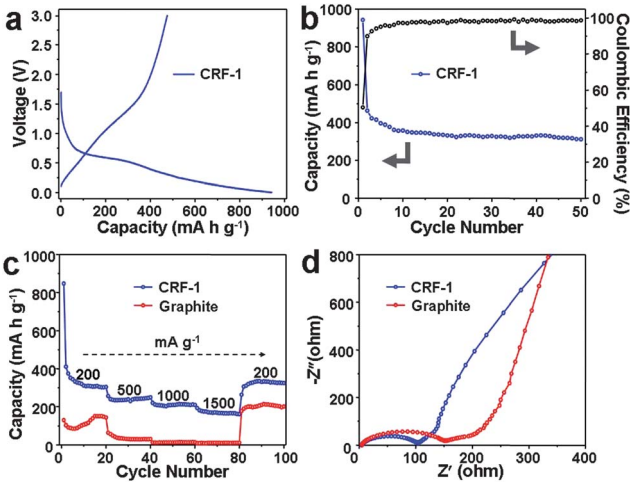

Fig. 7 The initial charge–discharge curves (a) of CRF-1 electrode at a current density of 100 mA g^{-1}; cycle performance (b) of CRF-1 at a current density of 100 mA g^{-1} between 0.005 and 3 V; rate performances (c) of CRF-1, CRF-4 and commercial artificial graphite at the different current densities; electrochemical impedance spectra (d) of CRF-1, CRF-4 and commercial artificial graphite obtained by applying a sine wave with amplitude of 5.0 mV over a frequency range of 100 kHz–0.01 Hz.

direction. It seems reasonable to speculate that the slim pores of the as-synthesized polymer (PRF-1 in Fig. 1c and d) are unable to bear the framework shrinkage during the carbonization process, resulting in the collapse of the mesostructures. To the best of knowledge, this is the first report on 1D carbon fibers with SEM and TEM visible organized mesostructures formed by hydrothermal synthesis.

Nanostructures self-assembled from surfactants provide a class of useful and versatile templates for generating nanomaterials in relatively large quantities. By varying the F127 concentration, a series of nanocarbons, denoted as CRF-*n* ($n = 2$, 3, 4, 5), were obtained. The detailed synthesis conditions are listed in Table 1. Indeed, the morphologies of the carbon products are remarkably affected by the amount of surfactant F127 used. As seen in Fig. 2a–c, by controlling the amount of F127 in the order of 0.0159, 0.0318, and 0.0636 mmol, the resultant nanocarbons markedly varied in shape from spheres to rods, and diameters from 250 nm to 140 nm. This is ascribed to, as increasing the concentration of F127, surfactant molecules spontaneously organize from spherical to rod-shaped micelles.[23–26] However, a further increase of the F127 concentration results in products with irregular morphologies (CRF-5 in Fig. 2d). Thus, the variation of the surfactant concentration determines the morphology of the self-assembled composite, under the driving force of the hydrogen-bond interaction between RF resin and F127 micelles. It should be noted that without using surfactant F127, crimson products composed of spherical particles were obtained. This is similar to the case of CRF-2 prepared with the lowest amount of F127. For clarity, the variations of as-synthesized nanocarbons in morphology and aspect ratio as a function of the amount of F127 used are compiled in Fig. 3.

Furthermore, CRF-2 and CRF-4 were characterized by HR-SEM and TEM. In the case of CRF-2, the HRSEM image (Fig. 4a) clearly confirms the spherical shape with a diameter of *ca.* 250 nm. Interestingly, one can see many linear pores (diameter of *ca.* 1 nm) along the axial surface of CRF-2, as seen from the TEM image in Fig. 4b, which may be attributed to the decomposition of F127 in the polymer matrix during the pyrolysis process. As shown in Fig. 4c, CRF-4 consists of nanorods with an average diameter of *ca.* 140 nm and remarkable long narrow grooves can be seen from the exposed surfaces. The TEM image further reveals the linear pores along the 1D growth direction.

It is known that HMT can decompose to NH_3 and formaldehyde during hydrothermal synthesis.[27] These *in situ* formed chemical molecules may influence the reaction kinetics, and thus the morphology and structure of the product. Comparison of the synthesis conditions between CRF-1 and CRF-4, clearly reveals that the amount of HMT can influence the morphology of the resultant carbon materials. With an increase in the amount of HMT, it can be speculated that the higher concentration of NH_3 may facilitate the reaction by forming more nuclei, thus resulting in a product with a reduced size. To testify the affect of the NH_3 concentration, 3.0 mmol ammonia instead of extra HMT was directly added to the solution, while keeping the other conditions the same as for CRF-4. As a consequence, some ring-shaped carbon products were formed (Fig. 5a). This phenomenon may

Table 2 A comparison of the electrochemical performance of carbon materials from the literature[a]

Type of material	C-rate/ mA g^{-1}	1st Reversible capacity/ mA h g^{-1}	Initial efficiency/ %	Cycles/reversible capacity/mA h g^{-1}	High C-rate/ mA g^{-1}	Reversible capacity/ mA h g^{-1}	Reference
Carbon nanofibers (CRF-1)	100	476	50.5	50/308	1500	160	This study
Carbon nanofibers	37.2 (0.1 C)	461	37	—	1860 (5 C)	200	37
Quadrangular carbon nanotubes	100	290	40	30/240	1000	136	40
Multiwalled carbon nanotubes	37.2 (0.1 C)	172	24	20/220	372 (1 C)	140	41
Carbon microtubes	25	480	47	20/443	1500	135	42
Hierarchical porous carbon	18.6	277.9	38.8	20/273	167.4	—	43
Mesoporous carbon-CNTs	37.2 (0.1 C)	910	52	20/786	1860 (5 C)	200	44
Aligned CNTs/graphene	30	—	—	40/290	3600	55	45
Amorphous carbon nanotubes	100	346	55	30/302	—	—	46
PAN-based carbon fiber	100	228	63	10/177	177	130	47
Carbon nanotube films	25	282	44	40/260	600	190	48

[a] 1 $C = 372$ mA g^{-1}.

be attributed to the changes in micelle morphology as a function of pH where ammonia is used in the synthesis process.[28,29] However, replacing extra HMT with 4.5 mmol of formaldehyde (keeping the other reaction conditions the same as for CRF-4), failed to generate a polymer gel (PRF-7, Fig. 5b inset). The representative dynamic light scattering (DLS) curves of PRF-7 and the original solution show that the average diameter of PRF-7 is only 18 nm larger than the corresponding original solution. These experiments demonstrate that only the *in situ* formed formaldehyde and ammonia decomposed from HMT have a significant impact on the formation of carbon nanofibers.

The thermal behavior of the polymer products corresponding to CRF-2 and CRF-4 was also investigated to monitor the degradation behavior by using thermogravimetry (TG; Fig. 6a) in a nitrogen atmosphere. A detectable weight loss step appears in the range of 300–400 °C, which is mainly attributed to the degradation of surfactant F127.[30,31] The differences in TG curves between the two samples are apparently ascribed to the amount of F127 used during the synthesis. The weight loss between 400 and 600 °C as well as above 600 °C coincides with the shrinkage of the carbon frameworks due to the thermal decomposition and condensation reactions.[32] This is a common phenomenon in carbon chemistry.

The N_2 sorption isotherm of the carbon nanofibers CRF-1 shows a quasi-type-I curve, which exhibits a transition between type-I and -IV curves (Fig. 6b). Interestingly, the isotherm exhibits a slight step in the relative pressure range of 0.10–0.40, characteristic of small mesopores. Such pores may be generated by the thermal decomposition of the surfactant F127. The hysteresis loop at higher pressure ($P/P_0 = 0.9$–0.997) reflects the inter-sample texture between the nanofibers. Generally, one would envisage that the N_2 sorption isotherms should be of type IV in shape with a type H2 hysteresis loop, which is typical for an ordered mesoporous material.[32,33] However, the resultant carbon nanofibers exhibit transitional type between a type-I and IV curve. This may be due to the slim diameter of the as-synthesized polymer, which is unable to bear the framework shrinkage during carbonization, leading to the collapse of mesostructures. Similar to CRF-1, the N_2 sorption isotherms of CRF-2 and CRF-4 exhibit similar behavior, showing quasi-type-I curves with a hysteresis loop at the high relative pressure (Fig. 6b). These hysteresis loops are an indication of the formed big pores among the closely packed carbon nanoparticles. As seen in the inset of Fig. 6b, the pore size distribution (PSD) of CRF-4, which was calculated using a density functional theory (DFT) model from the adsorption branch of the isotherms, shows the presence of small pores in the range of 0.75–3.3 nm. This is in good agreement with the SEM and TEM observations. Since sample CRF-1 and CRF-2 show similar pore size distributions to that of CRF-4, the PSD plots are thus not shown here. The BET surface areas of these carbon materials are in the range of 570–585 $m^2\ g^{-1}$ (Table 1), and the pore volumes are calculated to be *ca.* 0.30–0.35 $cm^3\ g^{-1}$. The 1D structures of CRF-1 with thin fiber diameters are considered to be propitious to Li-ion insertion and extraction, *i.e.*, facilitating the diffusion of Li-ions. Inspired by this, such a unique structure is expected to exhibit good electrochemical performances in LIBs. Thus, in the following study, we investigated the electrochemical performances of these nanocarbons as anode materials in rechargeable lithium-ion batteries.

Galvanostatic discharge (Li insertion)–charge (Li extraction) experiments were carried out to evaluate the electrochemical performance of carbon nanofibers. The electrochemical charge–discharge curves for the first cycle at a current density of 100 mA g^{-1} are shown in Fig. 7a. In the case of CRF-1, a first reversible capacity as high as 476 mA h g^{-1} is observed, higher than the theoretical capacity (372 mA h g^{-1}) of graphite.[34] Meanwhile, irreversible capacities occur in the CRF-1 electrode, which is common for porous carbon electrodes due to the formation of a solid electrolyte interface (SEI) film on the surface of carbons.[35–37] Similar to other non-graphitic carbon materials, there is no obvious plateau observed in the charge–discharge profiles of the samples, which is significantly different from that of graphite.[38,39] The slope between 0.8 and 0.5 V is generally ascribed to the formation of the SEI film that is ionically conducting and prevents further reaction of electrolyte and electron on the electrode surface.[34] The coulombic efficiency variation of CRF-1 is plotted as a function of the cycle number in Fig. 7b. The coulombic efficiency dramatically increases with discharge–charge cycles, reaching over 98%, after about 10 discharge–charge cycles. The cycling stability during the Li insertion/extraction processes is an important factor for successful application of carbon materials as electrodes for lithium-ion batteries. The specific capacity of CRF-1 after 50 cycles at a current density of 100 mA g^{-1} electrode is 308 mA h g^{-1}. Besides the high cycle stability, the as-synthesized carbon nanofibers also exhibit a promisingly good rate performance. Fig. 7c shows the variations of the reversible capacities of CRF-1 and commercial artificial graphite at different current densities. The electrodes were first cycled at 200 mA g^{-1} for 20 cycles, followed by cycling at current densities increasing stepwise to as high as 1500 mA g^{-1}. Cycling at a current density of 500 and 1500 mA g^{-1}, reversible capacities of approximately 249 and 160 mA h g^{-1} were obtained for CRF-1, respectively, much higher than that of commercial artificial graphite. This can be attributed to the unique morphology and nanoscale dimension of the carbon nanofibers, which facilitate the lithium ion transportation because of the reduction of the lithium ion diffusion length. To further understand the electrode kinetics of the carbon nanofibers during Li insertion, impedance spectroscopic studies were performed. Fig. 7d displays electrochemical impedance spectra of CRF-1 and commercial artificial graphite. The commercial artificial graphite anode has a larger charge transfer impedance than the carbon nanofibers anode, indicating that the charges transfer faster and easier at the electrode–electrolyte interface through the 1D nanocarbons. For clarity, a comparative table (Table 2) summarizes the electrochemical performance of carbon anodes for LIBs reported in the literature. The results confirm that the carbon nanofibers are promising anode materials for LIBs.

4 Conclusions

In conclusion, we have demonstrated a novel and facile synthesis of one-dimension nanocarbon materials based on the hydrothermal approach, using resorcinol and HMT as the monomers, and surfactant Pluronic F127 as the structure directing agent. The nanostructures and morphologies of the as-synthesized carbon materials were determined by the concentrations of F127 and HMT. Such a unique nanostructure of a 1D nanocarbon

material provides favorable transport kinetics for both lithium ions and electrons. As a result, a high reversible capacity, higher than 300 mA h g^{-1} and a high-rate capability, *ca.* 160 mA h g^{-1} at a current density of 1500 mA g^{-1}, have been achieved when 1D porous carbon nanomaterials are used as the anode material for lithium ion batteries. Overall, our results may provide new insights for the convenient synthesis of novel 1D porous carbon with desired nanostructures and architectures for the application of electrochemical energy conversion and storage.

Acknowledgements

The project was supported by NSFC (no. 21073026), the Program for New Century Excellent Talents in University of China (NCET-09-0254), the Fundamental Research Funds for the Central Universities, the Scientific Research Foundation for the Returned Overseas Chinese Scholars.

Notes and references

1 Y. Y. Liang, M. G. Schwab, L. J. Zhi, E. Mugnaioli, U. Kolb, X. L. Feng and K. Müllen, *J. Am. Chem. Soc.*, 2010, **132**, 15030.
2 G. W. Meng, F. M. Han, X. L. Zhao, B. S. Chen, D. C. Yang, J. X. Liu, Q. L. Xu, M. G. Kong, X. G. Zhu, Y. J. Jung, Y. J. Yang, Z. Q. Chu, M. Ye, S. Kar, R. Vajtai and P. M. Ajayan, *Angew. Chem., Int. Ed.*, 2009, **48**, 7166.
3 V. Vamvakaki, K. Tsagaraki and N. Chaniotakis, *Anal. Chem.*, 2006, **78**, 5538.
4 T. Chen, S. T. Wang, Z. B. Yang, Q. Y. Feng, X. M. Sun, L. Li, Z. S. Wang and H. S. Peng, *Angew. Chem., Int. Ed.*, 2011, **50**, 1815.
5 L. Ji and X. Zhang, *Nanotechnology*, 2009, **20**, 155705.
6 C. Kim, K. S. Yang, M. Kojima, K. Yoshida, Y. J. Kim, Y. A. Kim and M. Endo, *Adv. Funct. Mater.*, 2006, **16**, 2393.
7 C. Kim, B. T. N. Ngoc, K. S. Yang, M. Kojima, Y. A. Kim, Y. J. Kim, M. Endo and S. C. Yang, *Adv. Mater.*, 2007, **19**, 2341.
8 H. W. Liang, L. Wang, P. Y. Chen, H. T. Lin, L. F. Chen, D. He and S. H. Yu, *Adv. Mater.*, 2010, **22**, 4691.
9 H. J. Liu, X. M. Wang, W. J. Cui, Y. Q. Dou, D. Y. Zhao and Y. Y. Xia, *J. Mater. Chem.*, 2010, **20**, 4223.
10 W. Li, F. Zhang, Y. Q. Dou, Z. X. Wu, H. J. Liu, X. F. Qian, D. Gu, Y. Y. Xia, B. Tu and D. Y. Zhao, *Adv. Energy Mater.*, 2011, **1**, 382.
11 A.-H. Lu, G.-P. Hao, Q. Sun, X.-Q. Zhang and W.-C. Li, *Macromol. Chem. Phys.*, 2012, **213**, 1107.
12 H.-W. Liang, S. Liu and S.-H. Yu, *Adv. Mater.*, 2010, **22**, 3925.
13 M. Inagaki, Y. Yang and F. Kang, *Adv. Mater.*, 2012, **24**, 2547.
14 K. S. Yang, D. D. Edie, D. Y. Lim, Y. M. Kim and Y. O. Choi, *Carbon*, 2003, **41**, 2039.
15 F. Nitze, E. A. Hamad and T. Wågberg, *Carbon*, 2011, **49**, 1101.
16 M. Steinhart, C. Liang, G. W. Lynn, U. Gösele and S. Dai, *Chem. Mater.*, 2007, **19**, 2383.
17 D. Fujikawa, M. Uota, T. Yoshimura, G. Sakai and T. Kijima, *Chem. Lett.*, 2006, **35**, 432.
18 W. S. Chae, M. J. An, S. W. Lee, M. S. Son, K. H. Yoo and Y. R. Kim, *J. Phys. Chem. B*, 2006, **110**, 6447.
19 B. Z. Fang, M. Kim, S. Q. Fan, J. H. Kim, D. P. Wilkinson, J. Ko and J. S. Yu, *J. Mater. Chem.*, 2011, **21**, 8742.
20 T. Kyotani, L. F. Tsai and A. Tomita, *Chem. Mater.*, 1996, **8**, 2109.
21 K. Wang, W. Zhang, R. Phelan, M. A. Morris and J. D. Holmes, *J. Am. Chem. Soc.*, 2007, **129**, 13388.
22 H. W. Liang, W. J. Zhang, Y. N. Ma, X. Cao, Q. F. Guan, W. P. Xu and S. H. Yu, *ACS Nano*, 2011, **5**, 8148.
23 Q. Huo, D. I. Margolese, U. Ciesla, D. G. Demuth, P. Feng, T. E. Gier, P. Sieger, S. A. Firouzi, B. F. Chmelka, F. Schüth and G. D. Stucky, *Chem. Mater.*, 1994, **6**, 1176.
24 H. Ringsdorf, B. Schlarb and J. Venzmer, *Angew. Chem., Int. Ed. Engl.*, 1988, **27**, 113.
25 M. Li and J. Xue, *J. Colloid Interface Sci.*, 2012, **377**, 169.
26 P. Alexandridis and T. A. Hatton, *Colloids Surf., A*, 1995, **96**, 1.
27 B. H. Plesner and K. Hansen, *Carcinogenesis*, 1983, **4**, 457.
28 H. Shen, L. Zhang and A. Eisenberg, *J. Am. Chem. Soc.*, 1999, **121**, 2728.
29 M. Mao and S. R. Turner, *J. Am. Chem. Soc.*, 2007, **129**, 3832.
30 A.-H. Lu, B. Spliethoff and F. Schüth, *Chem. Mater.*, 2008, **20**, 5314.
31 S. Wang, W.-C. Li, G.-P. Hao, Y. Hao, Q. Sun, X.-Q. Zhang and A.-H. Lu, *J. Am. Chem. Soc.*, 2011, **133**, 15304.
32 Y. Meng, D. Gu, F. Zhang, Y. Shi, L. Cheng, D. Feng, Z. Wu, Z. Chen, Y. Wan, A. Stein and D. Zhao, *Chem. Mater.*, 2006, **18**, 4447.
33 G.-P. Hao, W.-C. Li, D. Qian, G.-H. Wang, W.-P. Zhang, T. Zhang, A.-Q. Wang, F. Schüth, H.-J. Bongard and A.-H. Lu, *J. Am. Chem. Soc.*, 2011, **133**, 11378.
34 R. Fong, U. Vonsacken and J. R. Dahn, *J. Electrochem. Soc.*, 1990, **137**, 2009.
35 Y.-S. Hu, P. Adelhelm, B. M. Smarsly, S. Hore, M. Antonietti and J. Maier, *Adv. Funct. Mater.*, 2007, **17**, 1873.
36 P. Adelhelm, Y.-S. Hu, L. Chuenchom, M. Antonietti, B. M. Smarsly and J. Maier, *Adv. Mater.*, 2007, **19**, 4012.
37 V. Subramanian, H. Zhu and B. Wei, *J. Phys. Chem. B*, 2006, **110**, 7178.
38 H. Zhao, J. Ren, X. He, J. Li, C. Jiang and C. Wan, *Electrochim. Acta*, 2007, **52**, 6006.
39 X. Li, S.-H. Yoon, K. Du, Y. Zhang, J. Huang and F. Kang, *Electrochim. Acta*, 2010, **55**, 5519.
40 J. Zhou, H. Song, B. Fu, B. Wu and X. Chen, *J. Mater. Chem.*, 2010, **20**, 2794.
41 C. Masarapu, V. Subramanian, H. Zhu and B. Wei, *Adv. Funct. Mater.*, 2009, **19**, 1008.
42 P. Meduri, J. H. Kim, H. B. Russell, J. Jasinski, G. U. Sumanasekera and M. K. Sunkara, *J. Phys. Chem. C*, 2010, **114**, 10621.
43 J. Yi, X. P. Li, S. J. Hua, W. S. Li, L. Zhoua, M. Q. Xua, J. F. Lei and L. S. Hao, *J. Power Sources*, 2011, **196**, 6670.
44 B. Guo, X. Wang, P. F. Fulvio, M. Chi, S. M. Mahurin, X.-G. Sun and S. Dai, *Adv. Mater.*, 2011, **23**, 4661.
45 S. Li, Y. Luo, W. Lv, W. Yu, S. Wu, P. Hou, Q. Yang, Q. Meng, C. Liu and H.-M. Cheng, *Adv. Energy Mater.*, 2011, **1**, 486.
46 J.-M. Shen, L. Xu, Y.-G. Liu, C.-L. Lu, W.-H. Hou and J.-J. Zhu, *Chem. Mater.*, 2008, **20**, 3034.
47 M. H. Kjell, E. Jacques, D. Zenkert, M. Behm and G. Lindbergh, *J. Electrochem. Soc.*, 2011, **158**, A1455.
48 S. Y. Chew, S. H. Ng, J. Wang, P. Novák, F. Krumeich, S. L. Chou, J. Chen and H. K. Liu, *Carbon*, 2009, **47**, 2976.

